Separation of C_2-C_4 Hydrocarbons from Methane by Zeolite MFI Hollow Fiber Membranes Fabricated from 2D Nanosheets

Byunghyun Min, Akshay Korde, Shaowei Yang, Youngjo Kim, Christopher W. Jones*, and Sankar Nair*

School of Chemical & Biomolecular Engineering, Georgia Institute of Technology, Atlanta, GA, 30332-0100, USA

*Corresponding authors: sankar.nair@chbe.gatech.edu, cjones@chbe.gatech.edu

Topical Heading: Separations

Keywords: natural gas processing, hollow fibers, membranes, nanosheets, zeolites

Abstract

Separation of higher hydrocarbons from methane is an important and energy-intensive operation in natural gas processing. We present a detailed investigation of thin and oriented MFI zeolite membranes fabricated from 2D MFI nanosheets on inexpensive α-alumina hollow fiber supports, particularly for separation of *n*-butane, propane, and ethane ("natural gas liquids") from methane. The present MFI membranes display high permeances and selectivities for C_2-C_4 hydrocarbons over methane, driven primarily by stronger adsorption of C_2-C_4 hydrocarbons. We study the separation characteristics under unary, binary, ternary and quaternary mixture conditions, including the pressure dependence. The membranes are highly effective in quaternary mixture separation at elevated feed pressures, for example allowing *n*-butane/methane separation factors of 170–280 and *n*-butane permeances of 710–2700 GPU in the 1-9 bar feed pressure range. Furthermore, we parametrize and apply multicomponent Maxwell-Stefan transport equations to predict the main trends in separation behavior over a range of operating conditions.

Introduction

Natural gas from shale resources is steadily replacing coal for power generation[1], and its demand is expected to grow substantially through 2040[2]. Shale gas is a multicomponent mixture containing methane (CH_4) as a major constituent (75-90%), substantial amounts of higher hydrocarbons such as ethane (C_2H_6), propane (C_3H_8), butanes (C_4H_{10}), and smaller quantities of higher hydrocarbons, CO_2, N_2, H_2S, and He [3]. Shale gas is usually classified as 'dry' or 'wet' gas according to the proportion of C_{2+} hydrocarbons [4], with 'wet' gas containing considerable amounts of C_{2+} hydrocarbons and less than 85% CH_4 [5] (**Table S1**). Therefore, a number of separation steps are necessary to remove contaminants (water, acid gases such as CO_2 and H_2S, and mercury) as well as the large quantities of C_{2+} hydrocarbons. The latter separation step is important for several reasons such as increasing the CH_4 content and fuel value, meeting the pipeline quality standards (950-1050 Btu/scf, dew point below -20°C), eliminating condensate formation [6], and valorizing the separated C_{2+} hydrocarbons as chemical feedstocks [7].

Conventionally, C_{2+} hydrocarbon recovery is performed by cryogenic distillation. Natural gas is expanded and then fractionated by a series of distillation columns (demethanizer, deethanizer, depropanizer, and debutanizer) [8]. These processes are highly energy-intensive, thus creating a large potential for energy-efficient and compact membrane separation technology for removing higher hydrocarbons from natural gas [9]. Conventional glassy and crystalline polymer membranes for gas separations are not suitable since they selectively permeate methane, whereas it is desired to permeate and remove the minority C_{2+} components through the membrane. Elastomeric and microporous polymer membranes have some selectivity for heavier hydrocarbons due to stronger adsorption, and hence membranes of materials such as poly(dimethylsiloxane) (PDMS) [10], PIM-1 [11], and poly(trimethyl-silyl-propyne) (PTMSP) [12] have been studied. Although

these membranes can be made at low cost, their permeability, selectivity, and low plasticization resistance [13] limit the potential for industrial applications.

It has long been suggested that inorganic zeolite membranes offer an attractive route for removing C_{2+} hydrocarbons (also referred to as natural gas liquids, NGLs) because of their much higher flux, high selectivity, and structural robustness [4,7,14-16]. MFI-type zeolite membranes possess strong adsorption-based selectivity for higher hydrocarbons, thereby allowing depletion of the NGL components and enriching the methane composition in the retentate stream [4,7,14-18]. However, zeolite membranes for hydrocarbon separations have been limited by their fabrication processes, that typically involve deposition of nanoparticle seed layers followed by hydrothermal growth into a polycrystalline membrane. These requirements create considerable difficulties in fabricating defect-free membranes on a large scale at sufficiently low cost. In recent years, it has been shown that the use of high-aspect-ratio (2D) MFI nanosheet coatings (instead of nanoparticle seed layers) can dramatically increase the quality of MFI membranes for hydrocarbon applications such as separation of xylene isomers or butane isomers [19-21]. However, the formation mechanism of these membranes still required the use of specially fabricated silica disk supports that are very expensive and not scalable at present. This is an important issue since the support has historically accounted for the majority of the cost of zeolitic membranes. Recently, we showed that high-quality 2D nanosheet-based MFI membranes could be made on inexpensive α-alumina hollow fibers that are produced by a standard spinning process without any surface engineering or modification steps [22]. These membranes displayed high separation performance for butane isomers. Based upon these encouraging prior findings, and the known adsorption selectivity of MFI for heavier hydrocarbons over methane, the present paper focuses on a detailed investigation of the separation of multicomponent (binary, ternary and quaternary) C_1-C_4 hydrocarbon mixtures by 2D nanosheet-

based MFI hollow fiber membranes over a range of mixture compositions and pressures. Our experimental investigation is complemented by detailed modeling of multicomponent permeation in MFI membranes by the Maxwell-Stefan approach.

Methods

The Supporting Information gives a complete account of the experimental details including membrane fabrication, characterization, and separation measurements; and the multicomponent Maxwell-Stefan transport modeling methods.

Results and Discussion

The fabrication and characterization of 2D nanosheet-based MFI hollow fiber membranes were carried out as reported by us in detail recently[22]. The **Supporting Information** (Experimental Details and **Table S2**) gives an account of these techniques. The main steps are the coating of 2D MFI nanosheets on α-alumina hollow fiber supports, followed by two (secondary and tertiary) hydrothermal steps to close the gaps between the nanosheets and form a continuous MFI membrane. A key factor is the use of two different structure directing agents (SDAs) in the secondary and tertiary hydrothermal steps. This strategy preserves the out-of-plane orientation of the zeolite MFI straight channels along the [0*k*0] crystallographic direction while effectively closing the gaps between the 2D nanosheets and limiting increase in membrane thickness. Since it is not our primary objective to elaborate upon our previous investigation of the membrane fabrication process[22], only a summary of membrane characterization data is shown here. **Figs. 1a-1b** show representative top-view and side-view SEM images of a membrane sample synthesized with 12 h secondary growth and 48 h tertiary growth. The membrane surface is continuous and non-faceted, due to in-plane filling of gaps between the nanosheets and suppression of faceted

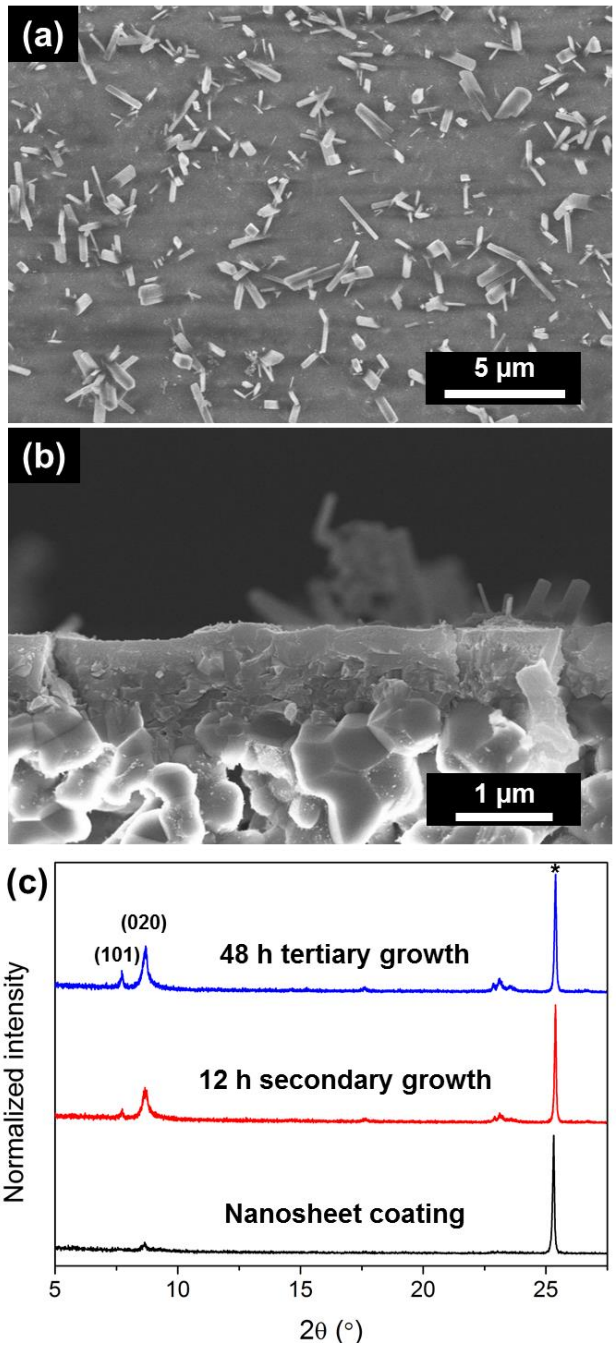

Figure 1. (a) Top-view and **(b)** cross-sectional SEM images of 2D nanosheet-based MFI hollow fiber membrane, **(c)** XRD patterns of the nanosheet coating, 12 h secondary growth membrane and 48 h tertiary growth membrane (* α-alumina support).

growth in the out-of-plane direction. Some discrete platelet-like crystals are observed to protrude from the membrane surface. These are thought to originate from misoriented growth in the central regions of the 2D MFI nanosheets [23], and also from secondary nucleation and crystal growth on

the membrane surface during tertiary growth. The membrane thickness was measured as 830 ± 200 nm. The XRD pattern of the final membrane (**Fig. 1c**) confirmed the excellent preservation of the (0*k*0) out-of-plane orientation throughout the fabrication process. These microstructural characteristics are in agreement with our previous work [22].

Detailed membrane permeation measurements were carried out by techniques described in the **Supporting Information** and **Fig. S1**. The selected components were based upon a balance between realistic feed conditions (*i.e.*, presence of the four main hydrocarbons of interest in the C_1-C_4 range) and the ease of producing feed mixtures over a wide pressure range using commercially available pre-mixed gas cylinders and pure components. Since our main focus is to examine the strong hydrocarbon adsorption effects, we do not include the small gas components such as CO_2, N_2, and H_2S. The mixtures also do not include *i*-butane or pentanes. The unary permeation properties of a 2D nanosheet-based MFI membrane at 298 K are shown in **Fig. S2** as a function of transmembrane pressure differential. The flux values are obtained by measuring the molar flow rate of each species in the sweep when it exits the hollow fiber membrane, and then dividing by the total membrane surface area. The partial pressure driving forces (required for calculating the permeances) are obtained as the difference between the feed-side partial pressure and the partial pressure measured in the exit permeate stream. Because the partial pressures of the hydrocarbons in the exit sweep gas are very small, there is no significant need to use arithmetic or logarithmic-averaged partial pressures on the permeate side. The unary permeances decrease in the order of increasing carbon number of the hydrocarbons. This is because the smaller hydrocarbons have higher intrinsic (Maxwell-Stefan) diffusivities in the MFI pores.

Separation data for a 10/90 vol% *n*-butane/methane mixture is shown in **Fig. 2a** as a function of transmembrane total pressure differential. Whereas methane permeates much faster

than *n*-butane in unary permeation, this effect is dramatically reversed in binary permeation. This is because of the strong competitive adsorption of *n*-butane in the MFI pores, thereby blocking adsorption and diffusion of methane. At higher zeolitic pore occupancies, the size entropy effect comes into play and boosts adsorption of methane to some extent [24], leading to lower (but still very high) *n*-butane/methane separation factor. The membrane exhibits excellent separation properties

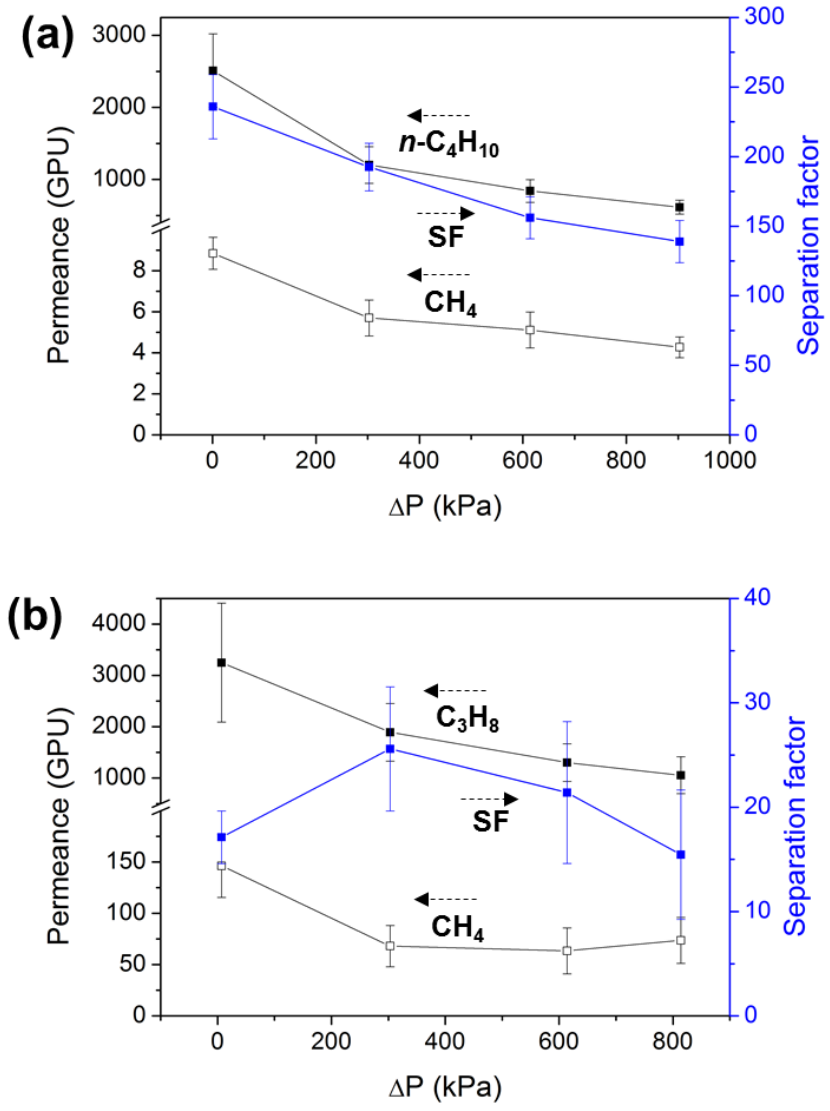

Figure 2. Permeances and separation factors at 298 K for **(a)** n-C_4H_{10}/CH_4 (10/90) binary mixture and **(b)** permeance and separation factor for C_3H_8/CH_4 (10/90) binary mixture, as a function of transmembrane pressure (ΔP). Error bars are obtained by measurements on three independently synthesized membrane samples.

over the entire pressure range (*n*-butane permeance of 2500-800 GPU and separation factors of 250-125), with a strong pressure dependence, as expected for an adsorption-controlled separation.

The propane/methane binary separation behavior at 298 K is shown in **Fig. 2b**. While high propane permeances (3200-1500 GPU) and good separation factors (15-25) are obtained, the pressure dependence of the separation factor and the methane permeance are substantially different from the *n*-butane/methane mixture. The separation factor shows a maximum at ΔP = 300 kPa and then decreases again. The permeance of methane initially decreases with increasing pressure, as expected, but it begins to rise again after 600 kPa, with a ~20 GPU increase between 600 kPa and 900 kPa. This behavior cannot be explained as being due to non-zeolitic (defect) pores [25], since a 20 GPU permeance contribution from defects should also have been observed from the same membranes in the *n*-butane/methane case of **Fig. 2a**, where the permeance of methane monotonically decreases. Rather, the above behavior is explained by the weaker adsorption of propane compared to *n*-butane. Propane requires a higher pressure than *n*-butane to saturate the MFI pores, and in this pressure region the separation factor increases with pressure as methane is progressively blocked. At higher pressures, methane is able to compete more effectively for adsorption with propane than with *n*-butane, resulting in a separation factor drop. A local maximum in the separation factor for binary ethane/methane mixtures at elevated feed pressure was also observed in a previous report[26]. Overall, the binary mixture measurements clearly show the potential of the 2D nanosheet-based MFI hollow fiber membranes for NGL removal.

Next, we measured multicomponent ternary and quaternary mixture permeation properties of the membranes. **Figs. 3a-3b** show the ternary *n*-butane/propane/methane (9/9/82 vol%) mixture separation behavior at ΔP = 0-900 kPa. Excellent separation factors for higher hydrocarbons are maintained over the entire range of pressures. The largest difference between the ternary and

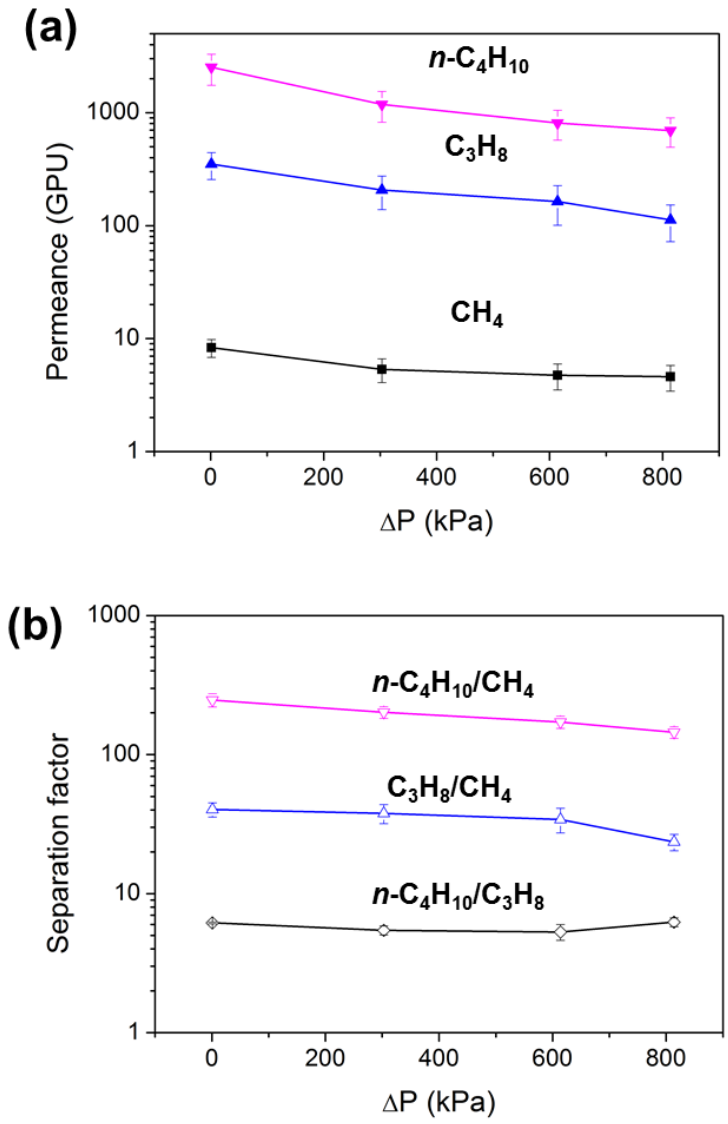

Figure 3. (a) Permeances and **(b)** separation factors observed for separation of *n*-C_4H_{10}/C_3H_8/CH_4 (9/9/82) ternary mixture as a function of transmembrane pressure (ΔP) at 298 K. Error bars are obtained by measurements on three independently synthesized membrane samples.

binary cases is in the behavior of propane. The presence of *n*-butane is effective in greatly suppressing the permeation of methane in a manner similar to the binary case (**Fig. 2a**). Although *n*-butane also suppresses the permeation of the weaker-adsorbing propane by almost an order of magnitude in comparison to **Fig. 2b**, the net effect is that the propane/methane separation factor in **Fig. 3b** (40-25 over the pressure range) is considerably enhanced over the binary case and no

longer displays a maximum with increasing pressure. It is also worth noting that the membranes show a significant ternary *n*-butane/propane separation factor of ~6 over the pressure range.

In the final set of multicomponent measurements, we evaluated the membrane performance using an 8/8/8/76 vol% *n*-butane/propane/ethane/methane quaternary mixture (**Figs. 4a-4b**). The permeances follow the same trend as the adsorption strength of the species, and the membranes are selective towards all the C_{2-4} hydrocarbons over methane. The *n*-butane/methane and propane/methane separation factors are further enhanced over the ternary case. The membranes have a significant ethane/methane separation factor of 4-3 over the pressure range. The membranes show good *n*-butane/propane and propane/ethane separation factors over the entire pressure range. Additionally, the membranes display high performance in multicomponent feed mixtures at higher pressures. The detailed permeation data show no signs of significant non-zeolitic (defect) permeation over a large range of lower to higher feed pressures, leading to maintenance of significant selectivity between different pairs of hydrocarbons over the entire pressure range. As a result, the same MFI zeolite membranes can potentially be used in multistage separations to debottleneck multiple distillation columns and produce enriched streams of all four hydrocarbons. The first stage (NGL removal from methane) would operate with higher-pressure feed gas (closer to the well-head pressure) to avoid recompression costs of the purified methane retentate product. On the other hand, the NGLs removed in the permeate of the first stage can be further separated at lower feed pressures without large recompression costs. The very high permeances of the MFI membranes enable this possibility as well.

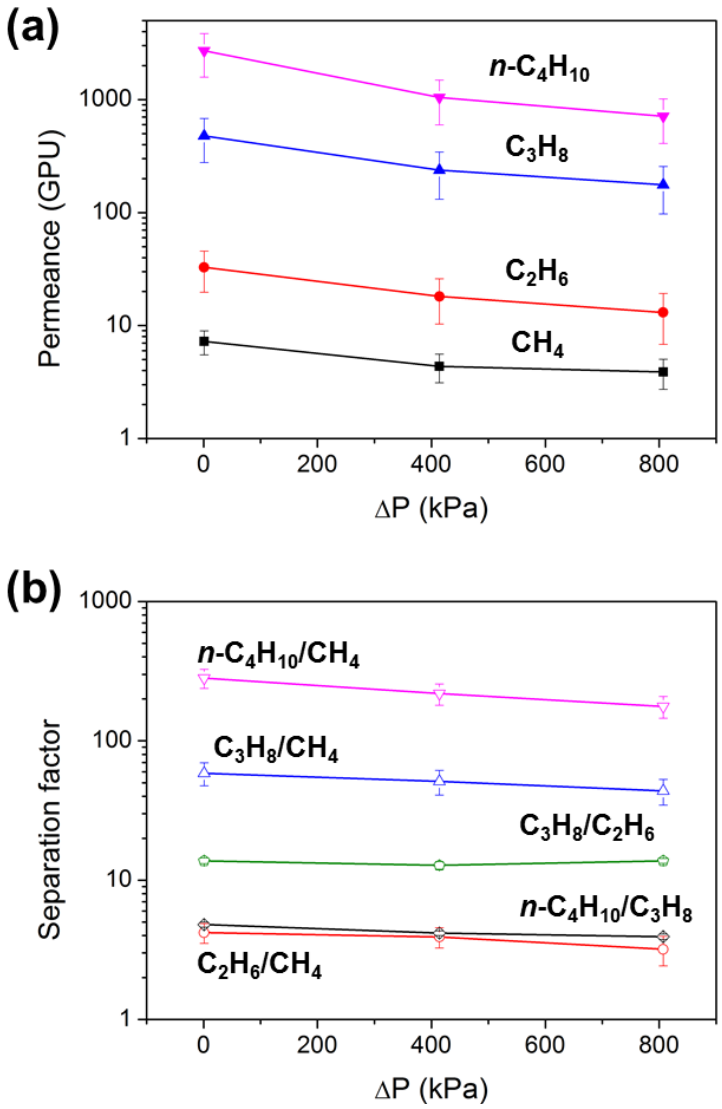

Figure 4. (a) Permeances and **(b)** separation factors observed for separation of a *n*-$C_4H_{10}/C_3H_8/C_2H_6/CH_4$ (8/8/8/76) quaternary mixture as a function of transmembrane total pressure differential (ΔP) at 298 K. Error bars are obtained by measurements on three independently synthesized membrane samples.

Figs. 5a-5b show a comparison of the permeation properties of all four hydrocarbons in unary and mixture permeation at a total transmembrane differential pressure, ΔP = 0 kPa (ethane is included only in the unary and quaternary cases). As compared to the permeance of propane in the unary and propane/methane binary mixtures, it permeates an order-of-magnitude slower in the presence of *n*-butane in the ternary and quaternary mixtures. Ethane and methane also behave

similarly, but to differing extents. The unary permeance of ethane is dramatically reduced by almost two orders of magnitude in mixture permeation, whereas methane permeation is reduced by nearly three orders of magnitude. On the other hand, the presence of propane and ethane has very little effect on *n*-butane permeance. The main feature of *n*-butane permeation is the dramatic

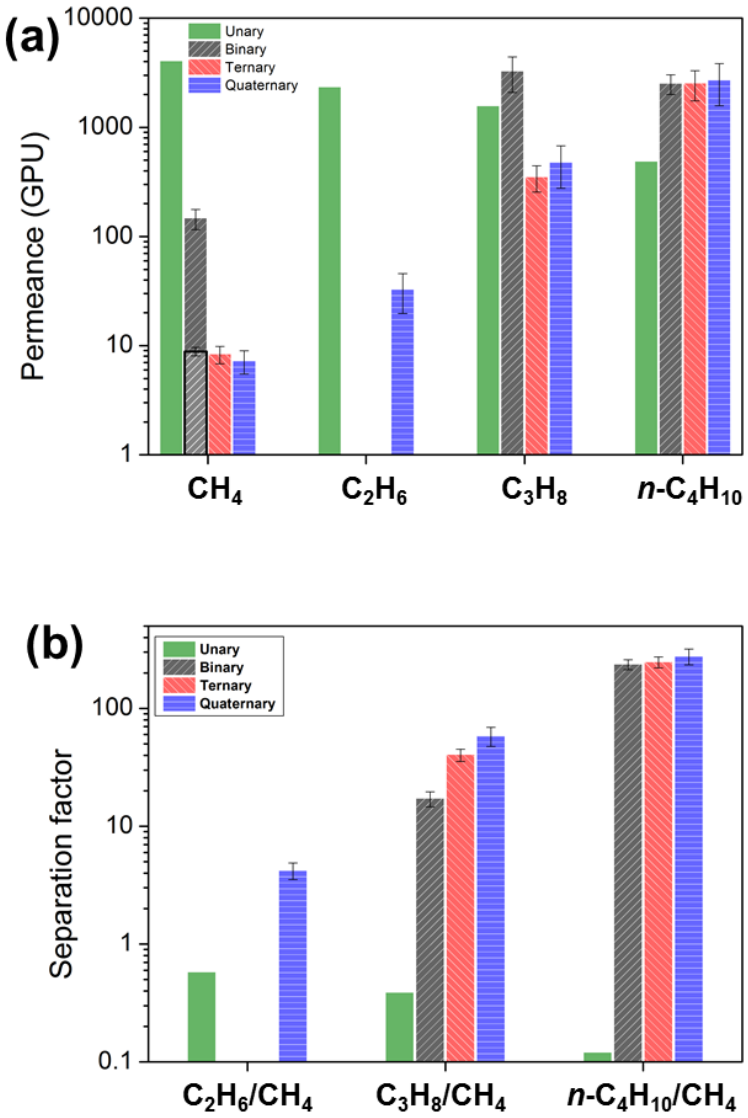

Figure 5. (a) Unary and multicomponent permeances in MFI membranes at 298 K and ΔP = 0 kPa for CH_4, C_2H_6, C_3H_8 and *n*-C_4H_{10}; and **(b)** corresponding separation factors of C_2H_6/CH_4, C_3H_8/CH_4 and *n*-C_4H_{10}/CH_4 at ΔP = 0 kPa. For unary permeation, ideal selectivities (ratios of unary permeances) are shown. **Legend:** Green = unary, Grey = binary (10/90 C_3H_8/CH_4 or *n*-C_4H_{10}/CH_4), Red = ternary (9/9/82 *n*-$C_4H_{10}/C_3H_8/CH_4$), Blue = quaternary (8/8/8/76 *n*-$C_4H_{10}/C_3H_8/C_2H_6/CH_4$). The CH_4 permeance for binary *n*-C_4H_{10}/CH_4 mixture is displayed with the border. The unary data is from a single membrane sample, whereas for the multicomponent data three independently fabricated samples were used.

permeance increase between the unary and mixture cases. In the unary case at 100 kPa, *n*-butane has near-saturated adsorption and the actual driving force would not increase proportionally at such a saturated pore occupancy. Thus, the permeance based on the pressure difference decreases and it is lower than the mixture case in which partial pressure of *n*-butane is lower[27]. The separation factors of the three heavier hydrocarbons over methane show a general increase from the unary to the quaternary case, since the overall increase in their proportion leads to further suppression of methane permeation. This effect of a multicomponent mixture system on the separation selectivity is more clearly observed when a sweep gas is used to maintain a low hydrocarbon chemical potential on the permeate side (as in this work). It was not observed in previous work [4], in which the ternary separation factors were lower compared to the binary mixtures in the absence of a sweep gas. Indeed, the adsorption-dominated separation performance of MFI membranes is highly influenced by the desorption conditions on the permeate side, as demonstrated previously[15]. **Fig. S3** shows the corresponding data at the highest pressures studied (ΔP = 800 or 900 kPa dependence on the mixture). Unary data were not measured at high pressures. The overall conclusions are similar to those discussed above.

To predict and understand the multicomponent permeation behavior in more detail, we modeled multicomponent transport in the MFI membranes with the Maxwell-Stefan (M-S) approach. Since there is a large range of possible feed compositions, pressures, and desorption conditions, a predictive multicomponent model can be very useful to ascertain the general trends in permeation behavior without need for extensive experimentation. This model could also be easily extended to add other components such as the small gases, butane isomers, or trace amounts of higher hydrocarbons (C_{5+}). Our objective here is not to make quantitatively accurate predictions over all the operating conditions by performing extensive parametrization. Rather, we take the

approach of making qualitatively useful predictions, employing unary adsorption (Configurational-bias Monte Carlo simulated data[28]) and experimental diffusion data to parametrize the M-S equations along with well-known theoretical approximations for multicomponent adsorption and exchange diffusion behavior. The **Supporting Information** contains a detailed account of the modeling methods and equations[29-33].

Detailed unary adsorption isotherm data are available for C_1-C_4 hydrocarbons in high-silica MFI zeolite at 300 K [28], which is close to the temperature of our membrane permeation measurements and allows the data to be used directly. **Fig. 6a** shows the fitted unary predictions with the dual-site Langmuir (DSL) model, revealing the large differences in adsorption behavior between the four components as a function of pressure. The DSL model was already shown to provide an excellent fit to the unary adsorption data[28], and the fitted adsorption parameters are listed in **Table S3**. The DSL model accounts for the presence of two different adsorption sites in the MFI pore structure, such as the channel intersections and the straight channels. There are several options available for multicomponent adsorption predictions. The ideal adsorbed solution theory (IAST) equations[34] are often used to predict the multicomponent adsorption isotherms. Although it is expected that the IAST model would predict the adsorption behavior of hydrocarbons in MFI quite well[35], its use in multicomponent M-S transport modeling is inconvenient due to its computational inefficiency. On the other hand, the extended dual-site Langmuir (EDSL) model is convenient due to its simple mathematical form that captures both the competitive and dual-site aspects of hydrocarbon adsorption in MFI. Initial trials showed that both methods predict identical trends in adsorption selectivity as a function of pressure and composition, although the numerical values of component uptakes and adsorptive separation factors can differ.

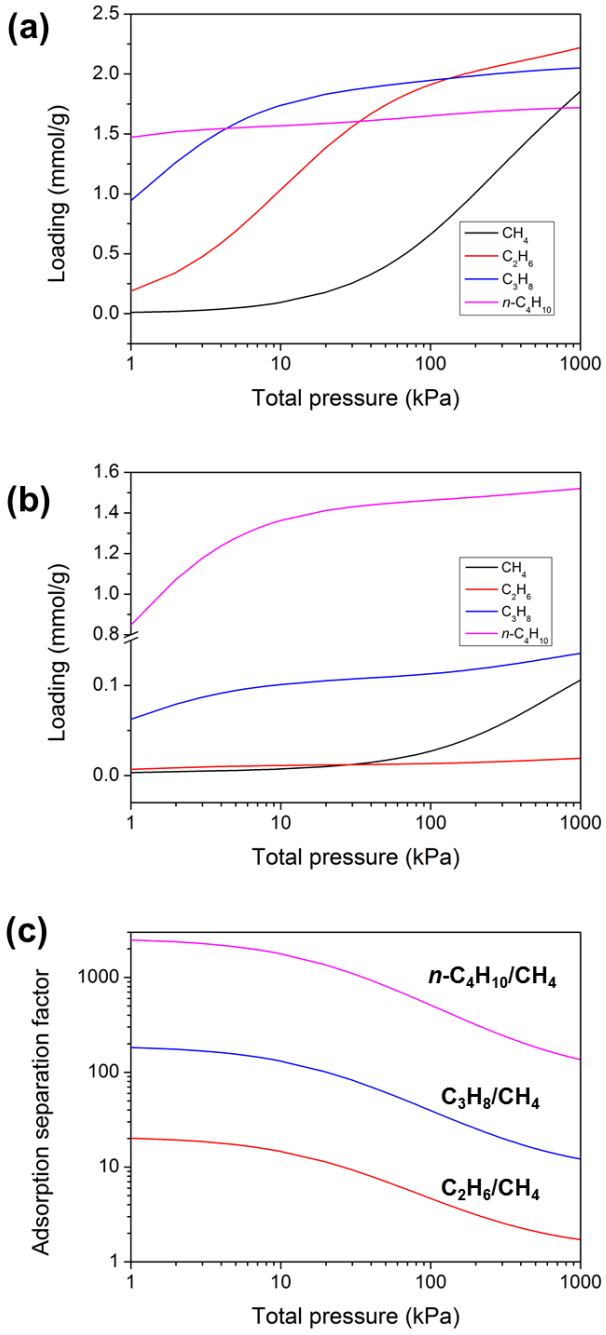

Figure 6. (a) Predictions of unary hydrocarbon adsorption in MFI at 300 K by the Dual-Site Langmuir model (fitted parameters in Table S3 [28]). Predictions of adsorption from a quaternary mixture (8/8/8/76 vol% n-C_4H_{10}/C_3H_8/C_2H_6/CH_4) by the Extended Dual-Site Langmuir model: **(b)** adsorption uptakes of each mixture component at different total pressures, and **(c)** corresponding adsorption separation factors.

Therefore, we proceeded to select the EDSL model for further calculations without undertaking any detailed comparison of IAST and EDSL predictions. For example, **Fig. 6b** shows the EDSL

prediction of quaternary mixture adsorption as a function of total pressure with the same 8/8/8/76 vol% mixture used for membrane permeation measurements. The EDSL model clearly predicts the large suppression of ethane and methane adsorption in the presence of propane and *n*-butane. The EDSL model also predicts the strong pressure dependence of quaternary mixture adsorption separation factors, as shown in **Fig. 6c**. The adsorption separation factor for a pair of components is defined as the ratio of the moles of the two components adsorbed in MFI, divided by the molar ratio of the components in the fluid phase. Similar to the observed quaternary mixture permeation trends, the adsorption separation factor decreases with increasing total pressure and the magnitude of the adsorption separation factor (of higher hydrocarbons over methane) follows the order of adsorption strength of the higher hydrocarbon.

Membrane permeation was modeled by the multicomponent M-S equations (see **Supporting Information** for details of the model formulation and assumptions). The required unary M-S diffusivity parameters were obtained by fitting our experimental unary permeation data (**Fig. S2**) to the M-S equation for each component, with the DSL model to describe the unary adsorption characteristics. **Fig. S4** shows these results. Considering the different approximations inherent in our approach, a reasonably good fit is obtained. As expected, the intrinsic M-S diffusivity of methane is much higher than that of the other components. With these diffusivity parameters and the multicomponent approximations listed in the Supporting Information, we can investigate a number of different aspects of multicomponent separations with the MFI membranes. **Fig. 7a** compares the M-S model predictions with experimental permeances and separation factors (of the three higher hydrocarbons over methane) for the quaternary mixture at $\Delta P = 800$ kPa. The M-S model correctly captures both the remarkable inversion of selectivity relative to unary

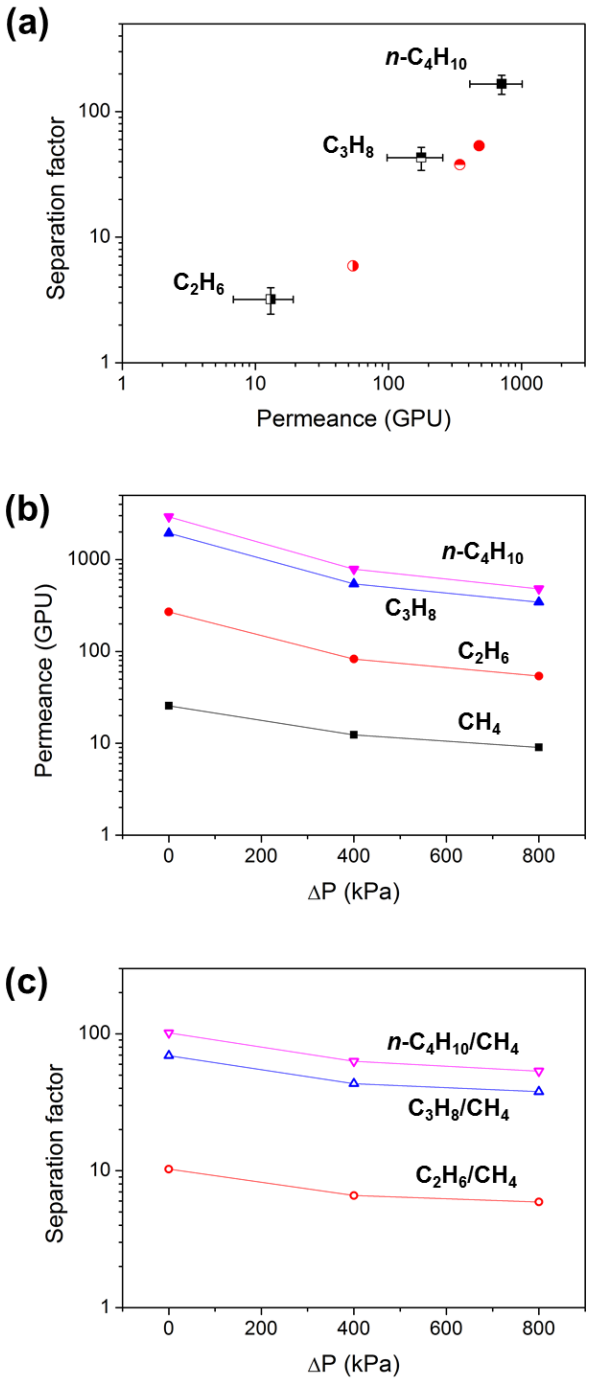

Figure 7. (a) Comparison of the Maxwell-Stefan predictions of permeances and separation factors for the quaternary mixture at ΔP = 800 kPa with the experimental results. **Legend:** Black = the experimental results, Red = the M-S model predicted values. Maxwell-Stefan predictions of the pressure dependence of **(b)** permeances and **(c)** separation factors.

permeation, as well as the changes in order of magnitude of permeances of each component.

Quantitative differences with the experimental data can be ascribed mainly to the limitations of

the Vignes relationship for predicting the counter-exchange coefficient, and the EDSL approximation of the adsorption behavior. It was previously reported that the flux of weaker-adsorbing species (here, methane and ethane) can be over-predicted by the Vignes relationship[36], leading to under-prediction of the *n*-butane separation factor over these species (as seen in **Fig. 7a**). Furthermore, the pressure-dependences of all the permeances and separation factors (**Figs. 7b-7c**) predicts the same trends as seen in **Fig. 4**. While quantitative discrepancies exist between the experimental and predicted values, the excellent qualitative correspondence supports the validity of the present model for examining the trends in separation performance.

We then proceeded to use the model to investigate several types of operating conditions. First, we modeled the effect of the permeate-side desorption conditions on the quaternary separation, by varying the sweep gas flow rate (**Figs. 8a-8b**). Upon reducing the sweep gas flow rate from 120 mL/min (60 mL/min is the value used in all the foregoing experiments and model calculations) to values as low as 10 mL/min, we find that the permeances of methane, ethane, and propane (and their corresponding mutual separation factors) are not significantly affected. These components do not have difficulty in desorbing on the permeate side even with increased concentrations on the permeate side (due to a reduction in sweep gas flow). On the other hand, the *n*-butane permeance shows a considerable decrease due to desorption limitations, upon lowering the sweep gas rate. Nevertheless, quite high *n*-butane permeances (> 300 GPU) and separation factors (~40) are still obtained at the lowest sweep flow rate modeled. Moreover, the model under-predicts the *n*-butane permeance (as discussed earlier) and the actual permeance may be considerably higher. Next, we examined the effect of reducing the total NGL content in the feed

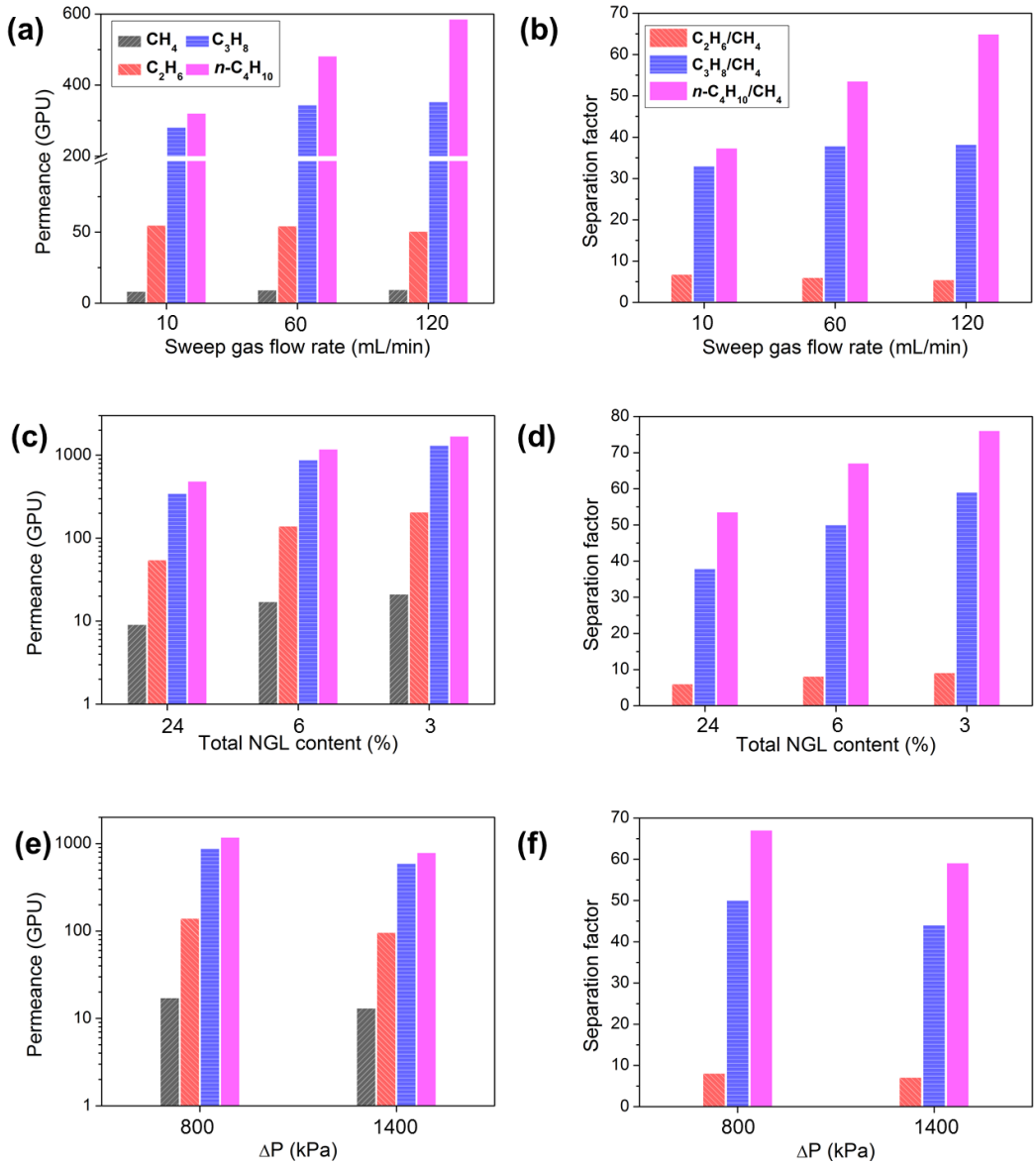

Figure 8. Predicted effect of sweep gas flow rate on **(a)** permeances and **(b)** separation factors in quaternary mixture separation at Δ P = 800 kPa. Predicted effect of the total NGL content (with fixed 1/1/1 ratio *n*-butane/propane/ethane) on **(c)** permeances and **(d)** separation factors at Δ P = 800 kPa. Predicted effect of operation at higher pressure (Δ P = 1400 kPa) for a 6% NGL feed (with fixed 1/1/1 ratio *n*-butane/propane/ethane) on **(e)** permeances and **(f)** separation factors. Legends for (c) and (e) are identical to the legend in (a). Legends for (d) and (f) are identical to the legend in (b).

stream at fixed ΔP = 800 kPa and sweep flow rate of 60 mL/min (**Figs. 8c-8d**). It is found that higher permeances and separation factors are obtained for all components at lower total NGL content. Even though the fluxes of NGL components would decrease somewhat because of the

reduced driving force, it appears that methane permeance can still be substantially suppressed and high separation performance can be achieved even at smaller concentrations of NGL components. Finally, for the case of a 2/2/2/94 vol% quaternary stream, we examine the effect of operating at a higher ΔP = 1400 kPa, since condensation at 6% total NGL is not a concern. As seen in **Figs. 8e-8f**, there is only a slight downward trend of permeances and selectivities with increasing pressure.

For all the above cases, the corresponding predicted fluxes (which are of greater practical interest than the permeances) are shown in **Fig. 9**. Several noteworthy observations can be made. First, a reduction in the sweep gas flow rate leads to a large decrease in the *n*-butane flux due to the inefficient permeate side desorption. Second, the C_2-C_4 hydrocarbon fluxes decrease when reducing the total NGL content in the feed stream. On the other hand, the methane flux increases due to the enhanced pressure gradient at lower total NGL content. Finally, for the 2/2/2/94 vol% quaternary stream, the higher operating feed pressure is found to increase the fluxes of all components, with the methane flux substantially affected due to the size entropy effect at higher pore occupancies. Despite a slight decrease in selectivities, a high flux at high pressure can compensate for such a loss of selectivities. Overall, these results have important implications for evaluating the performance and economic viability of MFI hollow fiber membranes in realistic natural gas processing. Better quantitative accuracy in M-S modeling may be achieved by the use of molecular simulations to provide multicomponent adsorption data as well as better estimates of counter-exchange diffusivities. Extension of the M-S model to include other components of shale gas (**Table S1**) would provide additional realistic performance predictions.

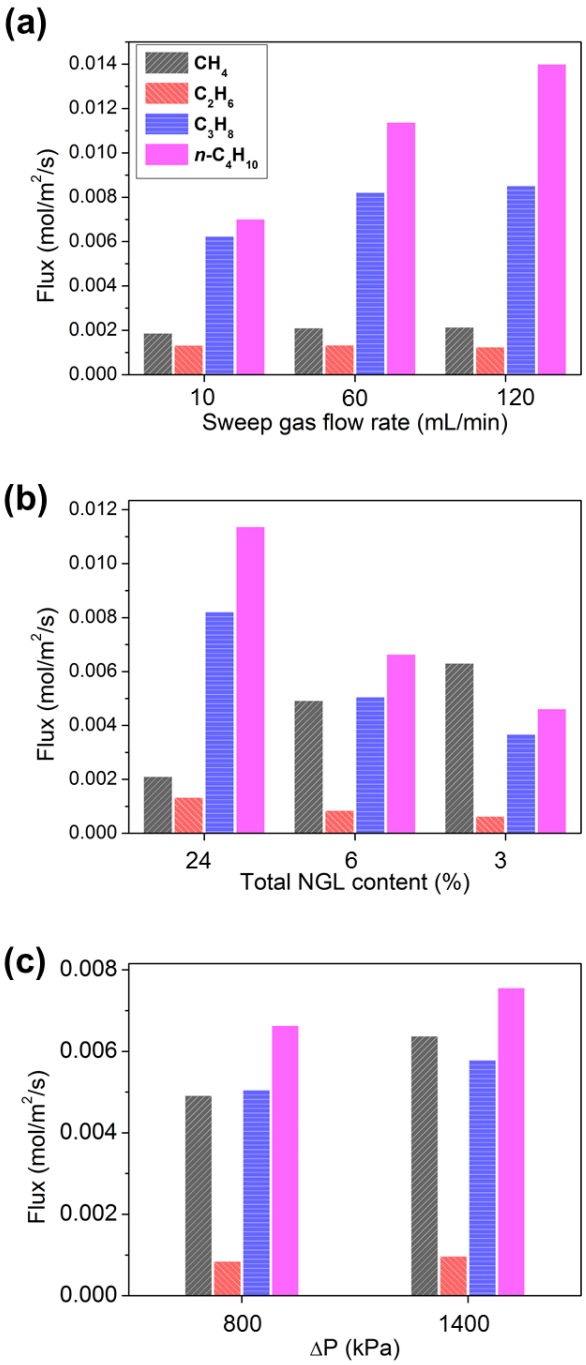

Figure 9. Predicted effect of **(a)** sweep gas flow rate, **(b)** total NGL content (with fixed 1/1/1 ratio *n*-butane/propane/ethane) at Δ P = 800 kPa on fluxes in quaternary mixture and **(c)** Predicted effect of operation at higher pressure (Δ P = 1400 kPa) for a 6% NGL feed (with fixed 1/1/1 ratio *n*-butane/propane/ethane) on fluxes in quaternary mixture. Legends for (b) and (c) are identical to the legend in (a).

Conclusion

In this study, 2D MFI-based hollow fiber membranes with favorable microstructure (thin and [0*k*0] out-of-plane orientation) were investigated for the removal of natural gas liquid (NGL) components (*n*-butane, propane, and ethane) from methane. The present membranes show excellent separation performance in the *n*-butane/propane/ethane/methane quaternary mixture at elevated feed pressures of up to 900 kPa. They are highly selective towards strongly adsorbing molecules such as *n*-butane and propane (e.g., *n*-butane/methane separation factor of 170 and *n*-butane permeance of 710 GPU at 900 kPa feed pressure) and also show selectivity for different pairs of hydrocarbons. As a result, such membranes could be used in a single stage for NGL removal from methane, and thereafter in a multistage cascade to fractionate the NGLs into streams rich in ethane, propane, and butane. Finally, we applied Maxwell-Stefan modeling to describe the multicomponent mixture transport behavior in a wide range of operating conditions (feed pressure, sweep gas flow rate and feed compositions), and demonstrated the potential utility of the present membranes in natural gas processing. The promising performance characteristics of the present membranes, combined with our concurrent advances in improving the scalability of zeolite membranes, could accelerate industrial applications of MFI zeolite membranes in hydrocarbon processing.

Acknowledgements

This work was supported by the National Science Foundation (CBET-1534179).

References

1. *February 2020 Monthly Energy Review*. U.S. Energy Information Administration; 2020.
2. *Annual Energy Outlook 2015*. Energy Information Agency;2015.
3. *Handbook of Natural Gas Transmission and Processing Principles and Practices.* Gulf Professional Publishing; 2015.
4. Yu L, Grahn M, Hedlund J. Ultra-thin MFI membranes for removal of C_{3+} hydrocarbons from methane. *J Membrane Sci.* 2018;551:254-260.
5. Conder MW, Lawlor KA. Production Characteristics Of Liquids-Rich Resource Plays Challenge Facility Design. *The American Oil & Gas Reporter*: National Publishers Group; 2014.
6. Baker RW. Future directions of membrane gas separation technology. *Ind Eng Chem Res.* 2002;41(6):1393-1411.
7. Arruebo M, Coronas J, Menendez M, Santamaria J. Separation of hydrocarbons from natural gas using silicalite membranes. *Sep Purif Technol.* 2001;25(1-3):275-286.
8. Park JH, Khan MS, Andika R, Getu M, Bahadori A, Lee M. Techno-economic evaluation of a novel NGL recovery scheme with nine patented schemes for offshore applications. *J Nat Gas Sci Eng.* 2015;27:2-17.
9. Scholes CA, Stevens GW, Kentish SE. Membrane gas separation applications in natural gas processing. *Fuel.* 2012;96(1):15-28.
10. Raharjo RD, Freeman BD, Paul DR, Sarti GC, Sanders ES. Pure and mixed gas CH4 and n-C4H10 permeability and diffusivity in poly (dimethylsiloxane). *J Membrane Sci.* 2007;306(1-2):75-92.

11. Thomas S, Pinnau I, Du NY, Guiver MD. Pure- and mixed-gas permeation properties of a microporous spirobisindane-based ladder polymer (PIM-1). *J Membrane Sci.* 2009;333(1-2):125-131.

12. Pinnau I, Toy LG. Transport of organic vapors through poly(1-trimethylsilyl-1-propyne). *J Membrane Sci.* 1996;116(2):199-209.

13. Schmeling N, Konietzny R, Sieffert D, Rolling P, Staudt C. Functionalized copolyimide membranes for the separation of gaseous and liquid mixtures. *Beilstein J Org Chem.* 2010;6:789-800.

14. Wohlrab S, Meyer T, Stohr M, Hecker C, Lubenau U, Ossmann A. On the performance of customized MFI membranes for the separation of n-butane from methane. *J Membrane Sci.* 2011;369(1-2):96-104.

15. Dragomirova R, Stohr M, Hecker C, Lubenau U, Paschek D, Wohlrab S. Desorption-controlled separation of natural gas alkanes by zeolite membranes. *Rsc Adv.* 2014;4(104):59831-59834.

16. Neubauer K, Dragomirova R, Stohr M, et al. Combination of membrane separation and gas condensation for advanced natural gas conditioning. *J Membrane Sci.* 2014;453:100-107.

17. Dragomirova R, Jorabchi MN, Paschek D, Wohlrab S. Operational Criteria for the Separation of Alkanes by Zeolite Membranes. *Chem-Ing-Tech.* 2017;89(7):926-934.

18. Geus ER, Vanbekkum H, Bakker WJW, Moulijn JA. High-Temperature Stainless-Steel Supported Zeolite (Mfi) Membranes - Preparation, Module Construction, and Permeation Experiments. *Microporous Mater.* 1993;1(2):131-147.

19. Jeon MY, Kim D, Kumar P, et al. Ultra-selective high-flux membranes from directly synthesized zeolite nanosheets. *Nature.* 2017;543(7647):690-694.

20. Kim D, Jeon MY, Stottrup BL, Tsapatsis M. para-Xylene Ultra-selective Zeolite MFI Membranes Fabricated from Nanosheet Monolayers at the Air-Water Interface. *Angew Chem Int Edit.* 2018;57(2):480-485.

21. Agrawal KV, Topuz B, Pham TCT, et al. Oriented MFI Membranes by Gel-Less Secondary Growth of Sub-100 nm MFI-Nanosheet Seed Layers. *Adv Mater.* 2015;27(21):3243-3249.

22. Min B, Yang SW, Korde A, Kwon YH, Jones CW, Nair S. Continuous Zeolite MFI Membranes Fabricated from 2D MFI Nanosheets on Ceramic Hollow Fibers. *Angew Chem Int Edit.* 2019;58(24):8201-8205.

23. Kim D, Shete M, Tsapatsis M. Large-Grain, Oriented, and Thin Zeolite MFI Films from Directly Synthesized Nanosheet Coatings. *Chem Mater.* 2018;30(10):3545-3551.

24. Krishna R. Diffusion of binary mixtures across zeolite membranes: Entropy effects on permeation selectivity. *Int Commun Heat Mass.* 2001;28(3):337-346.

25. Poshusta JC, Noble RD, Falconer JL. Temperature and pressure effects on CO2 and CH4 permeation through MFI zeolite membranes. *J Membrane Sci.* 1999;160(1):115-125.

26. van de Graaf JM, van der Bijl E, Stol A, Kapteijn F, Moulijn JA. Effect of operating conditions and membrane quality on the separation performance of composite silicalite-1 membranes. *Ind Eng Chem Res.* 1998;37(10):4071-4083.

27. van de Graaf JM, Kapteijn F, Moulijn JA. Methodological and operational aspects of permeation measurements on silicalite-1 membranes. *J Membrane Sci.* 1998;144(1-2):87-104.

28. Krishna R, Baur R. Modelling issues in zeolite based separation processes. *Sep Purif Technol.* 2003;33(3):213-254.

29. van den Broeke LJP, Bakker WJW, Kapteijn F, Moulijn JA. Binary permeation through a silicalite-1 membrane. *Aiche J.* 1999;45(5):976-985.

30. Kapteijn F, Moulijn JA, Krishna R. The generalized Maxwell-Stefan model for diffusion in zeolites: sorbate molecules with different saturation loadings. *Chem Eng Sci.* 2000;55(15):2923-2930.

31. Krishna R, Paschek D. Separation of hydrocarbon mixtures using zeolite membranes: a modelling approach combining molecular simulations with the Maxwell-Stefan theory. *Sep Purif Technol.* 2000;21(1-2):111-136.

32. Kapteijn F, Bakker WJW, Zheng GH, Moulijn JA. Temperature-Dependent and Occupancy-Dependent Diffusion of N-Butane through a Silicalite-1 Membrane. *Microporous Mater.* 1994;3(3):227-234.

33. Vignes A. Diffusion in Binary Solutions - Variation of Diffusion Coefficient with Composition. *Ind Eng Chem Fund.* 1966;5(2):189-199.

34. Simon CM, Smit B, Haranczyk M. pyIAST: Ideal adsorbed solution theory (IAST) Python package. *Comput Phys Commun.* 2016;200:364-380.

35. Krishna R, Baur R. Analytic solution of the Maxwell-Stefan equations for multicomponent permeation across a zeolite membrane. *Chem Eng J.* 2004;97(1):37-45.

36. Krishna R, Li S, van Baten JM, Falconer JL, Noble RD. Investigation of slowing-down and speeding-up effects in binary mixture permeation across SAPO-34 and MFI membranes. *Sep Purif Technol.* 2008;60(3):230-236.